ISSN 0973-3450 (Print)
JUC Vol. 15(6), 54-65 (2019). Periodicity 2-Monthly
ISSN 2319-8036 (Online)

JOURNAL OF ULTRA CHEMISTRY
An International Open Free Access Peer Reviewed Research Journal of Chemical Sciences and Chemical Engineering
website:- www.journalofchemistry.org
Estd. 2005

Understanding the effect of terminal electron-deficient group on the performance of small molecule acceptor in organic solar cells

ASIF MAHMOOD[1,2]

[1]CAS Key Laboratory of Nanosystem and Hierarchical Fabrication, CAS Center for Excellence in Nanoscience, National Center for Nanoscience and Technology, Beijing 100190, P. R. (China)
[2]University of Chinese Academy of Sciences, Beijing 100049, P. R. (China)
Corresponding Author Email:- asifmahmood023@gmail.com
http://dx.doi.org/10.22147/juc/150601

Acceptance Date 30th November, 2019, Online Publication Date 05th December, 2019

Abstract

End groups plays very important role to tune the properties and performance of small molecule acceptors. In this study, theoretical analysis was performed to find the reason why two similar molecule differ in end-group showed much different performance in organic solar cells. 1,1-dicyanomethylene-3-indanone based small molecule acceptor (DC-IDT2Tz) showed higher transition dipole moment as compare with malononitrile based small acceptor (MN-IDT2Tz). DC-IDT2Tz showed lower exciton binding energy as compare to MN-IDT2Tz. As well as, DC-IDT2Tz showed lower reorganization energy and higher transfer integral as compare with that of MN-IDT2Tz. All the theoretical descriptors are explaining reason behind the higher efficiency of DC-IDT2Tz. Studying theoretical parameters can help to check the performance of organic semi-conductor before synthesis. This work will be helpful for experimental scientists to screen the compounds and to select best one for synthesis.

Key words: Organic solar cells; small molecule acceptors; PTB7-Th; exciton binding energy.

Introduction

Recently, bulk heterojunction (BHJ) organic solar cells (OSCs) has gained huge fame. Organic solar cells possess distinct advantages such as easy synthesis of active layer materials, flexibility, light weight and large area fabrication. More importantly, properties of active layer materials (donor and acceptor) can be easily tuned[1,2]. Fullerene derivatives have remained most successful electron-accepter material for long time[3-6]. However, they also possess few non-avoidable the drawbacks such low light absorption ability, limited chance electroptical properties, expensive synthesis and film brittleness[7-9].

Therefore, designing of alternative acceptors is ultimate need.

From recent few years, performance of non-fullerene acceptors (NFAs) has been significantly improved. Comparative to competitors, they have unique advantages such as easily tunable chemical structures, low cost synthesis and strong absorption in broad range[10-14]. Non-fullerene small molecule acceptors are designed by suitable combination of electron-rich and electron-deficient groups. These groups controls the energy levels of target molecules[11,15-18].

Indaceno[2,1-b:6,5-b]dithiophene (IDT) based acceptors are among the successful non-fullerene small molecule acceptors. In 2018, our group has reported a small molecule acceptor (DC-IDT2Tz) based on IDT as middle building block, thiazole as π-spacer and 1,1-dicyanomethylene-3-indanone (DC) as terminal electron-deficient group[10]. The solution processed BHJ OSCs based on PTB7-Th:DC-IDT2Tz showed a PCE of 5.81%. From getting inspiration from this study, another small molecule acceptor was synthesized by using malononitrile as terminal electron-deficient unit. Structures of both small molecule acceptors are given in Figure 1. However, newly synthesized small acceptor (MN-IDT2Tz) showed lower performance (3.95%). A detail computational analysis was performed to find the reason behind it. So, that avoid the synthesis of unsuccessful materials and give a design rule future work.

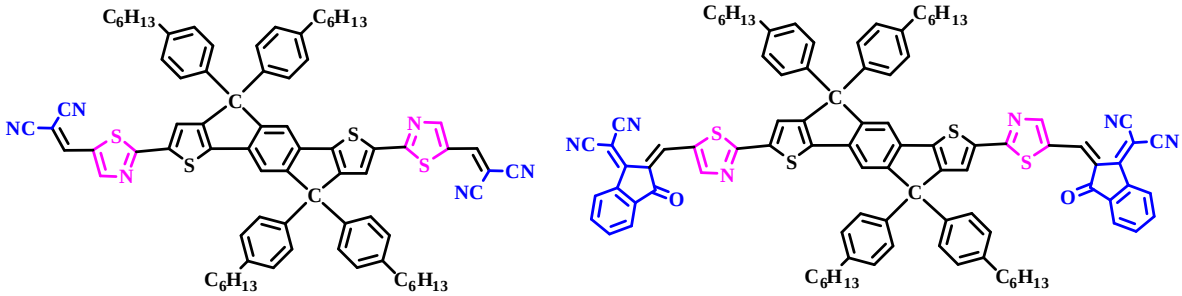

Figure 1. Structure of MN-IDT2Tz and DC-IDT2T.

2. Experimental and Computational detail

2.1. Experimental detail

2.1.1. Materials

Unless stated otherwise, all the solvents and chemical reagents used were obtained commercially (derthon chemical company, China) and were used without further purification.

2.1.2. Produce :

Synthesis of compound 3 :

A two necked round-bottom flask was added compound **1** (265mg, 1.38mmol), compound **2** (813mg, 0.66mmol) and toluene (60mL). The mixture was deoxygenated with nitrogen for 20 minutes, and then $Pd(PPh_3)_4$ (35mg, 0.03mmol) was added. The mixture was refluxed for 48 hours and then cooled to room temperature. 150 mL of KF saturated solution was added and stirred for 30 minutes. The mixture was extracted with CH_2Cl_2 (3×100 mL). The organic phase was dried over anhydrous $MgSO_4$. After removing the solvent, the residue was purified by column chromatography on silica gel with CH_2Cl_2/ethyl acetate (33:1) as an eluent yielding a yellow solid (830 mg, 89%). 3: ^{1}H NMR (400 MHz, $CDCl_3$):δ = 10.0(s,2H),

8.32(s, 2H), 7.60(s,2H), 7.22-7.18 (m, 8H), 7.14-7.11 (m, 10H), 2.60 (m, 8H), 1.61-1.57 (m, 8H), 1.32-1.29 (m, 24H), 0.9 (m, 12H) ppm.

Synthesis of MN-IDT2Tz :

3 (575 mg, 0.51 mmol), malononitrile (136 mg, 2.05 mmol), and basic aluminum oxide (2.2 g) in anhydrous toluene (60 mL) was heated to 110 °C and stirred for 2h. The reaction mixture was then cooled to room temperature, and the basic aluminum oxide residue was removed by filtration and thoroughly washed with toluene. The solvent of the filtrate was removed by rotary evaporation, and the crude product was purified via column chromatography over SiO_2 with CH_2Cl_2 as the eluent. Yielding MN-IDT2Tz as a violet solid (200 mg, 48%). MN-IDT2Tz: ^{1}H NMR (400 MHz, $CDCl_3$): δ = 8.15(s,2H),7.86 (s, 2H), 7.62(s,2H), 7.55 (s, 2H), 7.17-7.10 (m, 16H), 2.59-2.56 (m, 8H), 1.61-1.57 (m, 10H), 1.32-1.29 (m, 22H), 0.88-0.85 (m, 12H) ppm. MS (MALDI-TOF-MS): Calculated for $C_{78}H_{76}N_6S_4$, 1224.5, found: 1225.2.

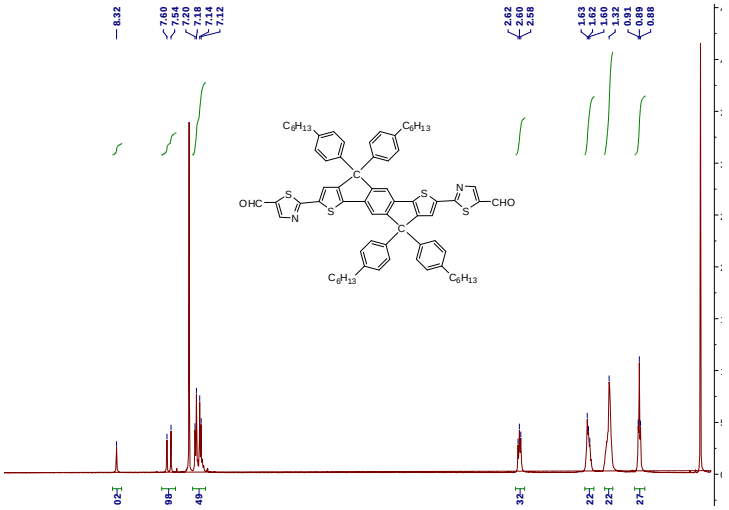

Figure 2. ^{1}H NMR spectra of compound 3.

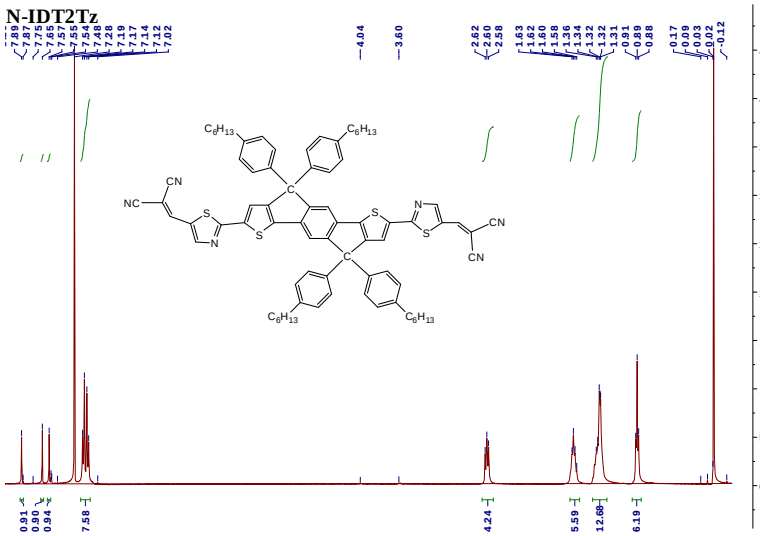

Figure 3. ^{1}H NMR spectra of MN-IDT2Tz

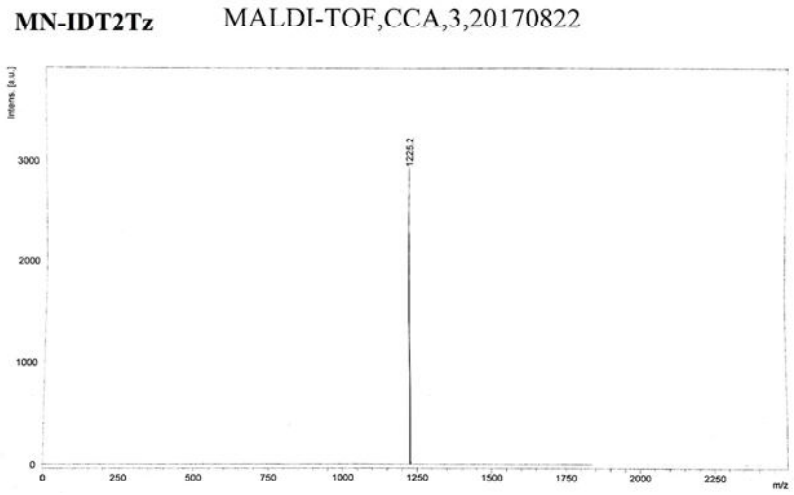

Figure 4. Mass Spectrum of MN-IDT2Tz

2.1.3. Methods

^{1}H NMR spectra was obtained using a Bruker Advance III 400 (400 MHz) nuclear magnetic resonance (NMR) spectroscope. UV-vis absorption spectra were tested on Lambda 950 (Perkin Elmer Instruments Co. Ltd, USA). Cyclic voltammetry (CV) was done on an electrochemical workstation with working electrode Pt plate, counter electrode Pt wire and standard calomel electrode (SCE) as reference electrode. The CV curves were recorded versus the potential of SCE, which was calibrated by the ferrocene-ferrocenium (Fc/Fc^+) redox couple, which absolute energy level is 4.8 eV below vacuum.

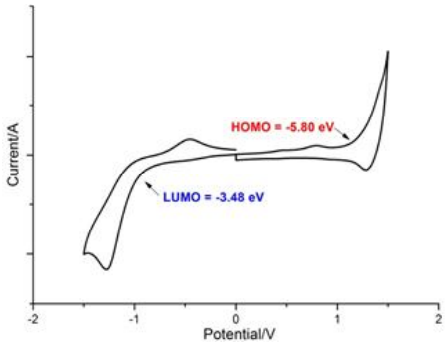

Figure 5 cyclic voltammogram of MN-IDT2Tz.

2.1.4. Fabrication and characterization of photovoltaic cells :

Device fabrication and photovoltaic characterization were done according to reported method[10].

2.2. Computational detail :

Single molecule geometries were optimized using Gaussian 09 at ωB97XD/6-31G(d,p) level of theory. Success of optimization was checked by absence of imaginary frequency. Binding energy of dimmers, transition dipole moment and electron coupling (transfer integral) were also calculated at same level of theory. Ionization potential (IP), electron-affinity (EA) and optical gap (E_g^o) were calculated using M06/6-31G(d,p). Reorganization energy (λ) was calculated using B3LYP/6-31G(d,p). To simplify the calculations, alkyl chains were replaced by a methyl group.

3. Results and Discussion

3.1. Synthesis, electronic and optical properties :

Synthesis steps of MN-IDT2Tz are given in scheme 1. In first step, Stille coupling reaction between 2-bromothiazole-5-carbaldehyde and compound 1 resulted the intermediate compound 3. Knoevenagel condensation reaction of malononitrile with compound 3 afforded the final product MN-IDT2Tz in high yield.

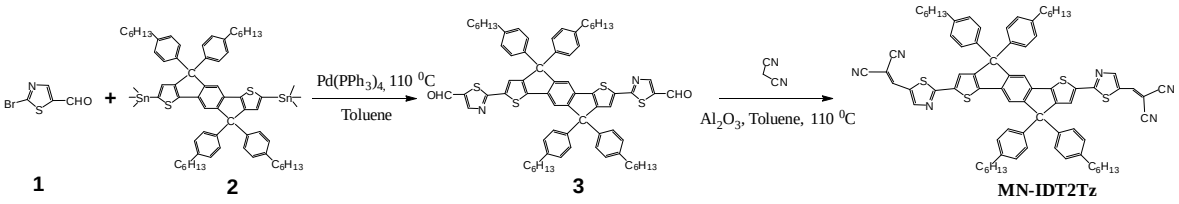

Scheme 1. Synthetic route of MN-IDT2Tz.

The electrochemical behavior of DC-IDT2T was studied using cyclic voltammetry (CV). MN-IDT2T exhibited irreversible reduction wave and quasireversible oxidation wave shown in Figure S4. HOMO and LUMO energy levels are calculated from onset oxidation and reduction potentials. HOMO and LUMO values are -5.80 and -3.48 eV respectively. Band gap is 2.32.

UV/vis spectra of MN-IDT2Tz in chloroform solution (10^{-5} M) and in thin solid film show in Figure 6. It showed strong absorption in the 450–650 nm region with a maximum extinction coefûcient of 0.90×10^{5} $M^{-1}cm^{-1}$ at 578 nm. In thin film, MN-IDT2T showed broader absorption band relative to that in solution but absorption intensity is lower.

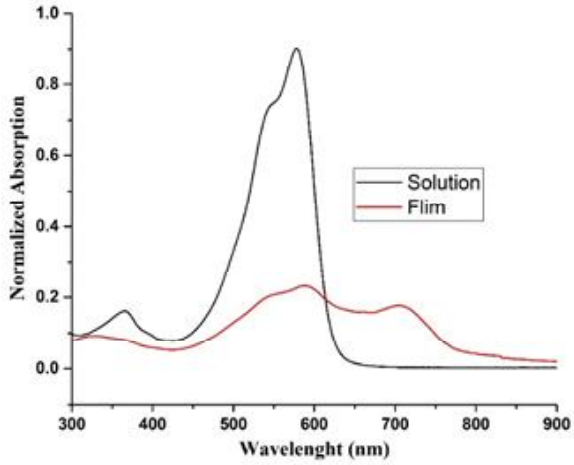

Figure 6. UV-vis absorption spectra of MN-IDT2Tz in chloroform solution and in thin film.

3.2. Photovoltaic performance and film morphology characterization :

Organic solar cells were fabricated using PTB7-Th:MN-IDT2Tz as active layer material. The typical current–voltage curves of the OSCs under the illumination of 100 mW cm^{-2} AM are shown in Figure 7. The device showed broad photocurrent response in 300–800 nm, which should be attributed to the absorptions of both PTB7-Th and MN-IDT2Tz. The maximum EQE value of PTB7-Th:MN-IDT2Tz reached 50% at 600 nm.

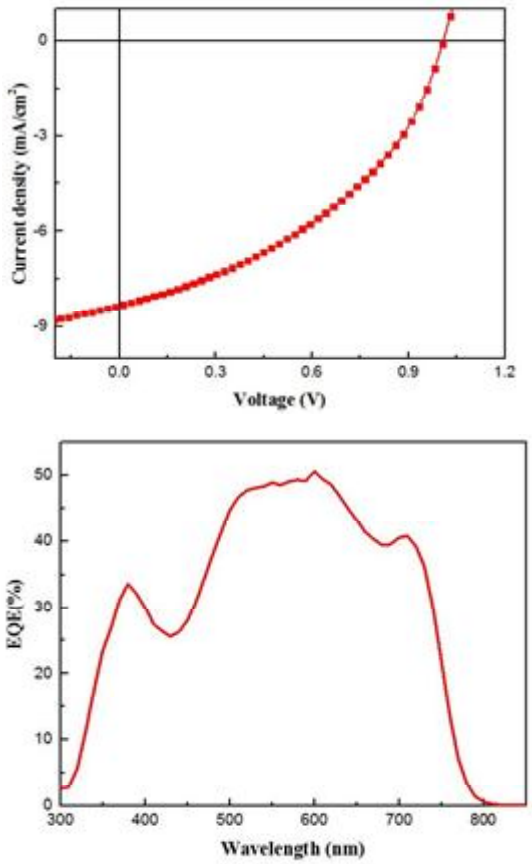

Figure 7. J–V curves (a) and EQE spectra (b) of PTB7-Th:MN-IDT2Tz.

A detail study was performed to understand effect of different factors on photovoltaic parameters. We have used three solvents. From Table 1, it is clear that chlorobenzene (CB) is much better choice than chloroform (CF) and o-dichlorobenzene (ODCB). Solvent change significantly altered the all parameters. It is also known that the weight ratios of donor and acceptor in active layers play important roles in the performance of OSCs. So, active layers of solar cells were made by using diûerent weight ratios of PBT7-Th and MN-IDT2Tz. It was found that a weight ratio of 1:1.5 showed the maximum photovoltaic response (3.95%). Effect of donor/acceptor ratio is not so prominent. It affected all the parameters. A balance combination of photovoltaic parameters provided top PCE value. Thermal annealing showed a significant alteration in photovoltaic performance (Table 3). Device showed maximum PCE of 3.75% at 100 °C. Further increase of temperature did not show beneficial effect and PCE underwent small decrease.

Table 1. Effect of solvent on photovoltaic performance

Solvent	V_{OC} (V)	J_{SC} (mA/cm^2)	FF	PCE
CF	0.95	4.29	31.29	1.46
CB	0.98	7.09	33.99	2.70
O-DCB	1.01	3.95	42.19	1.92

Table 2. Effect of donor: acceptor ratio (PTB7-Th:MN-IDT2Tz) on photovoltaic performance

D/A	V_{OC} (V)	J_{SC} (mA/cm^2)	FF	PCE
1.5:1	0.98	7.15	43.78	3.47
1:1	0.99	7.65	44.30	3.81
1:1.5	1.01	8.35	41.60	3.95
1:2	1.01	7.97	40.06	3.63

Table 3. Effect of annealing temperature on photovoltaic performance

Annealing (°C)	V_{OC} (V)	J_{SC} (mA/cm^2)	FF	PCE (%)
No	0.96	7.57	33.03	2.72
80	0.97	8.78	36.14	3.50
100	0.97	8.97	38.01	3.75
120	0.97	8.90	37.04	3.63
140	0.99	8.44	38.12	3.61

Overall comparison of photovoltaic performance of MN-IDT2Tz and DC-IDT2Tz is given in Table 4.

Table 4. Photovoltaic performance of MN-IDT2Tz and DC-IDT2Tz

Acceptor	V_{OC} (V)	J_{SC} (mA/cm^2)	FF	PCE
PTB7-Th:DC-IDT2Tz	0.82	10.81	65.54	5.81*
PTB7-Th:RD-IDT2Tz	1.01	8.35	41.60	3.95

* taken from reference[10]

Given that the morphologies of blend films are directly related to device performances. Grazing incident X-ray difiraction (GIXD) and atomic force microscopy (AFM) were used to evaluate the film morphology. AFM height and corresponding phase images are shown in Figure 8. From figure it can be seen that the surface of PTB7-Th:MN-IDT2Tz is uniform and smooth with root-mean-square (rms) surface roughness values of 1.15 nm. That may be beneficial for exciton dissociation and charge transport.

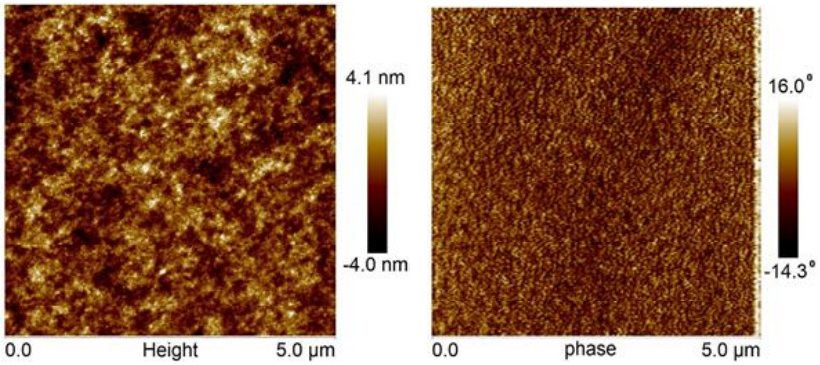

Figure 8. AFM height and phase images of the PTB7-Th:MN-IDT2Tz

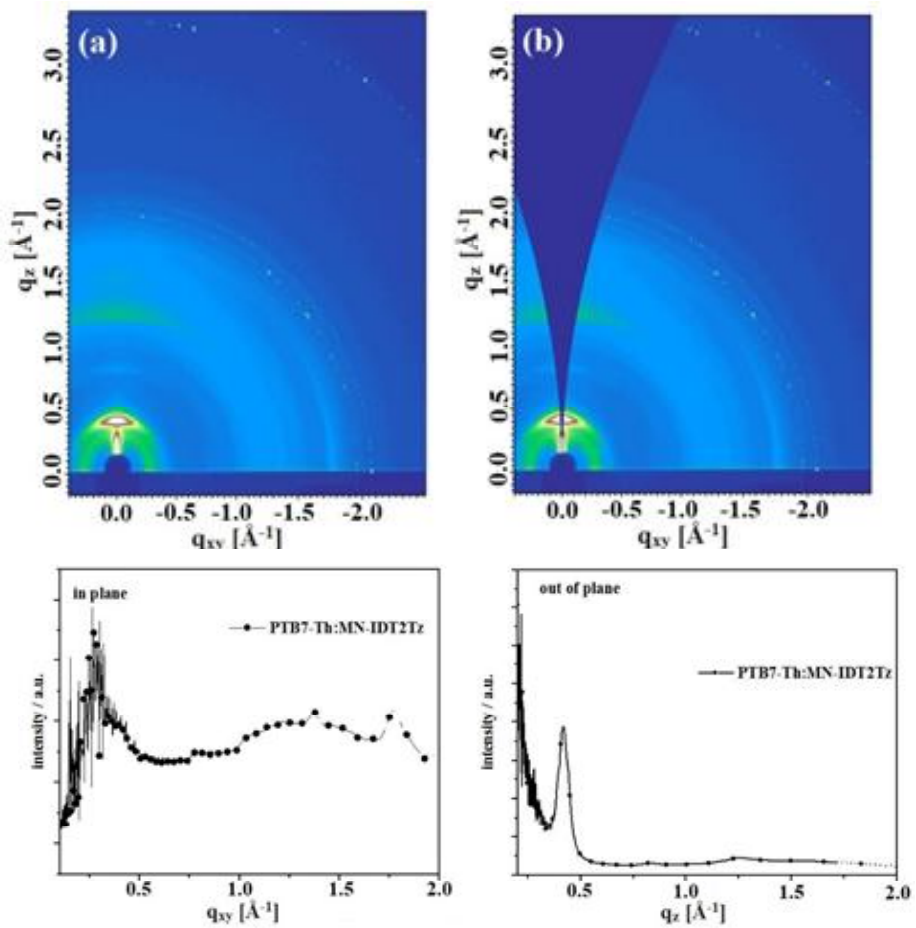

Figure 9. 2D patterns of grazing-incidence wide-angle X-ray scattering (GIWAXS) measured on pure film of PTB7-Th (a) and BHJ films of PTB7-Th:MN-IDT2Tz (b) Out-of-plane and in-plane line cuts from respective GIWAXS patterns for PTB7-Th:MN-IDT2Tz.

The microstructures of the optimized pure and blend ûlms were further characterized by grazing-incidence wide-angle X-ray scattering (GIWAXS). GIWAXS provides understanding of crystallinity and orientation of donor as well as acceptor in blend film. GIWAXS patterns of neat PTB7-Th and PTB7-Th:MN-IDT2Tz blend and the corresponding line-cuts of are shown in Figure 9. PTB7-Th showed a (100) difiraction peak in in-plane (IP) direction at 0.45 Å^{-1} and a (010) diûraction peak in the out-of-plane (OOP) direction at 1.25 Å^{-1}. After being blended with MN-IDT2Tz, chain packing behavior remained same. π–π stacking difiraction in OOP direction indicates Face-on orientation. The face-on orientation is beneûcial for vertical charge transport and corresponding OPV performance.

The electron and hole mobilities of the devices were estimated from space-charge-limited current (SCLC) method (Figure 10). The structures of hole-only and electron-only devices were ITO/ PEDOT:PSS/ PTB7-Th:MN-IDT2Tz/Au and ITO/TIPD/PTB7-Th:MN-IDT2Tz/Al respectively. Devices exhibited a hole mobility of 3.89×10^{-5} cm^{2}V^{-1}S^{-1} and an electron mobility of 2.48×10^{-8} cm^{2}V^{-1}S^{-1}. However, the electron mobility of DC-IDT2Tz is higher (4.96×10^{-7} cm^{2}V^{-1}s^{-1}).

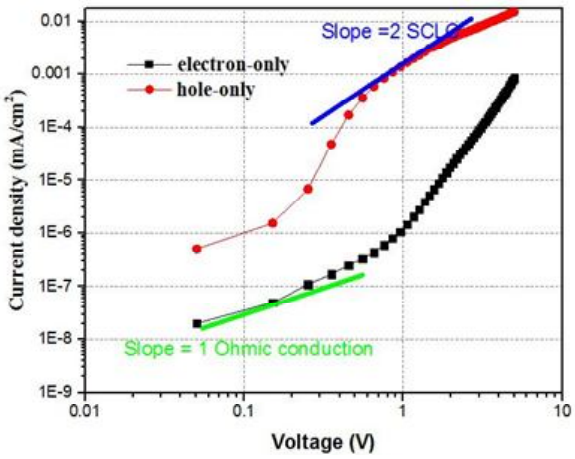

Figure 10. Typical J–V curves based on the hole-only and electron-only devices devices based PTB7-Th:MN-IDT2Tz.

The change of terminal electron-deficient group from 1,1-dicyanomethylene-3-indanone (DC-IDT2Tz) to malononitrile (MN-IDT2Tz) has significantly reduced performance. So, a detail theoretical calculations were performed to find reason behind it.

3.3. Intrinsic Charge Transfer and exciton binding energy :

Many oligomers[19-26] and polymers[23, 27-35] showed intramolecular charge-transfer (ICT) character due to the presence of multiple building blocks with different electron affinities. Insertion of atoms or groups with high electron-affinity extract charge from other parts of molecule. As mention in above section, DC-IDT2Tz showed more disperse charge distribution. This will result a higher local electron density gradient and will lead to higher transition dipole moment ($\Delta\mu_{ge}$). Compared with MN-IDT2Tz, DC-IDT2Tz showed higher $\Delta\mu_{ge}$. That can lead to more polarized exciton and is more likely to produce a better separated hole and electron, which experiences less coulombic attraction and, hence, is more likely to become free charge carriers. Electronic transition from ground state to first excited states makes a dominant contribution to the light absorption in the long-wavelength range. So, increase of electron density gradient is efficient way to increase the light absorption ability of small molecule acceptors.

Exciton dissociation is most critical part in the working mechanism of organic solar cells. The electrostatic forces that holds the electron and hole together is called binding energy. The fundamental transport gap and the optical gap are used to find the exciton binding energy:

$$E_b = E_g^t - E_g^o \Rightarrow (1)$$

In above equation, E_g^o is optical gap and it is the excitation energy of the first singlet excited state (S1). Following equation was used to determine the fundamental transport gap (E_g^t):

$$E_g^t = IP - EA \Rightarrow (2)$$

where the ionization potential (IP) is calculated as energy difference between cationic and neutral state, electron affinity (EA) is calculated as the energy difference between the neutral state and anionic state.

$$\mathrm{IP} = \mathrm{E}_{+} - E_0 \Rightarrow (3)$$

$$\mathrm{EA} = \mathrm{E}_0 - E_{-} \Rightarrow (4)$$

As compare to MN-IDT2Tz, DC-IDT2Tz showed higher ionization potential (IP) and electron-affinity (EA) values. E_g^t values decrease because of more increase in EA as compare to IP. On overall basis, DC-IDT2Tz showed lower exciton binding energy as compare with MN-IDT2Tz.

Table 5. Dipole moment difference between first excited state and ground state ($\Delta\mu_{ge}$), Ionization potential IP, electron affinity EA, band gap (E_g^t), optical gap (E_g^o) and exciton binding energy.

Molecule	$\Delta\mu_{ge}$ (Debye)	IP (eV)	EA (eV)	E_g^t (eV)	E_g^o (eV)	E_b (eV)
MN-IDT2Tz	0.1256	6.14	2.67	3.49	1.98	1.51
DC-IDT2Tz	0.1609	6.25	2.80	3.45	2.15	1.30

Local π–π stacking between terminal acceptor units of FREAs has been well studied[36-39]. DFT was used to calculate the optimized molecular geometries of dimers at the uB97XD/6-31G(d,p) level. The corresponding intermolecular binding energies were calculated by correction of the basis set superposition error (BSSE) according to the literature method[39] (Figure 11). DC- IDT2Tz showed bimolecular binding energy of -26.56 kcal/mol, while MN-IDT2Tz showed bimolecular binding energy of -21.74 kcal/mol. Benzene of 1,1-dicyanomethylene-3-indanone is responsible for better intermolecular π–π interactions between DC-IDT2Tz molecules. However, rhodanine do not has benzene ring as well as has steric hindrance result from ethyl group, so it led lower π–π interactions between MN-IDT2Tz molecules. The results are demonstrating that the terminal electron-deficient unit can effectively regulate the local intermolecular π–π interactions, thus influences the electron mobilities and impact the eventual photovoltaic performance.

Figure 11. Intermolecular binding energies of dimmer of MN-IDT2Tz and DC-IDT2Tz

3.4. Reorganization energy and transfer integral :

Reorganization energy and transfer integral are two important descriptors for charge mobility. Lower reorganization energy and higher transfer integral lead to higher charge mobility. Reorganization energy for electron transfer can be calculated using following equation.

$$\lambda_{-} = E_0(\mathrm{Q}_{-}) - E_0(\mathrm{Q}_0) + E_{-}(\mathrm{Q}_0) - E_{-}(\mathrm{Q}_{-}) \Rightarrow (5)$$

where $E_0(Q_0)$ and $E-(Q-)$ are the corresponding energies of optimized neutral and anionic structures. $E_0(Q-)$ is the neutral energy of the optimized anionic structure of the molecule, and $E-(Q_0)$ is the anionic energy of the optimized neutral structure.

Transfer integrals were directly calculated from frontier molecular orbitals (FMOs)[40, 41].

$$t_{e/h} = \left\langle \phi_{LUMO/HOMO}^{0,site1} \middle| F^0 \middle| \phi_{LUMO/HOMO}^{0,site2} \right\rangle$$
$$= \left\langle \phi_{LUMO/HOMO}^{0,site1} \middle| h_{core} \middle| \phi_{LUMO/HOMO}^{0,site2} \right\rangle + \sum_{l(occ)} \left(\left\langle \phi_{LUMO/HOMO}^{0,site1} \phi_l^0 \middle| \phi_{LUMO/HOMO}^{0,site2} \phi_l^0 \right\rangle - \left\langle \phi_{LUMO/HOMO}^{0,site1} \phi_{LUMO/HOMO}^{0,site2} \middle| \phi_l^0 \phi_l^0 \right\rangle \right) \Rightarrow (6)$$

Where $\phi_{LUMO/HOMO}^{0,site1}$ and $\phi_{LUMO/HOMO}^{0,site2}$ correspond to the HOMOs and LUMOs of two consecutive molecules when there is no contact between adjacent molecules. F^0 is the Fock operator with unperturbed molecular orbitals for the dimer of a fixed pathway. The reorganization energy is directly associated with the geometrical distortion of a chemical substance. Reorganization energy of DC-IDT2Tz (0.158 eV) was much lower than that of MN-IDT2Tz (0.181 eV). As well as DC-IDT2Tz showed higher transfer integral (0.192 eV) that is much higher than that of MN-IDT2Tz (0.178 eV). That is clearly indicating the higher electron-mobility for DC-IDT2Tz.

Table 6. Reorganization Energy (λ) and Transfer Integral (t)

Acceptor	λ (eV)	t (eV)
MN-IDT2Tz	0.181	0.178
DC-IDT2Tz	0.158	0.192

4. Conclusions

In summary, DC-IDT2Tz showed more disperse charge distribution and more local electron density gradient as compare with MN-IDT2Tz. DC-IDT2Tz showed higher transition dipole moment as compare with MN-IDT2Tz. DC-IDT2Tz showed lower exciton binding energy as compare to MN-IDT2Tz. As well as, DC-IDT2Tz showed lower reorganization energy and higher transfer integral as compare with that of MN-IDT2Tz. All the theoretical descriptors are explaining reason behind the higher efficiency of DC-IDT2Tz.

5. Scope of future work :

This work will be helpful for experimental scientists to screen the compounds and select best one for synthesis. This study will pave path for further development. Studying theoretical parameters can help to judge the performance of materials before synthesis. These parameters further can be validated to enhance their usefulness.

6. Acknowledgements

Asif Mahmood sincerely acknowledge the CAS-TWAS President's Fellowship Program for providing the financial support.

7. Abbreviations

PTB_7-Th	Poly[4,8-bis(5-(2-ethylhexyl)thiophen-2-yl)benzo[1,2-b;4,5-b']dithiophene-2,6-diyl-alt-(4-(2-ethylhexyl)-3-fluorothieno[3,4-b]thiophene-)-2-carboxylate-2-6-diyl)]
DC-IDT2Tz	A molecule based on Indaceno[2,1-b:6,5-b]dithiophene (IDT) as middle part, thiazole (Tz) as π-spacer and 1,1-dicyanomethylene-3-indanone (DC) as terminal electron-deficient group
MN-IDT2Tz	A molecule based on Indaceno[2,1-b:6,5-b]dithiophene (IDT) as middle part, thiazole (Tz) as π-spacer and malononitrile (MN) as terminal electron-deficient group
J–V curve	current–voltage curve
EQE	External quantum Efficiency
PCE	Power conversion efficiency
V_{OC}	open circuit voltage
J_{SC}	Short-circuit current
FF	Fill factor
AFM	Atomic force microscopy

References

1. Mahmood, A., *et al., Recent progress in porphyrin-based materials for organic solar cells.* Journal of Materials Chemistry A, *6(35),* p. 16769-16797 (2018).
2. Tang, A., *et al., Design of Diketopyrrolopyrrole (DPP)-Based Small Molecules for Organic-Solar-Cell Applications.* Advanced Materials, *29(2),* p. 1600013 (2017).
3. Yao, H., *et al., Molecular Design of Benzodithiophene-Based Organic Photovoltaic Materials.* Chemical Reviews, *116(12),* p. 7397-7457 (2016).
4. Lin, Y. and X. Zhan, *Oligomer Molecules for*

Efficient Organic Photovoltaics. Accounts of Chemical Research, *49(2)*, p. 175-183 (2016).

5. Lin, Y., Y. Li, and X. Zhan, *Small molecule semiconductors for high-efficiency organic photovoltaics*. Chemical Society Reviews, *41(11)*, p. 4245-4272 (2012).
6. Mohajeri, A. and A. Omidvar, *Fullerene-based materials for solar cell applications: design of novel acceptors for efficient polymer solar cells - a DFT study*. Physical Chemistry Chemical Physics, *17(34)*, p. 22367-22376 (2015).
7. He, Y. and Y. Li, *Fullerene derivative acceptors for high performance polymer solar cells*. Physical Chemistry Chemical Physics, *13(6)*, p. 1970-1983 (2011).
8. Li, C.-Z., H.-L. Yip, and A.K.Y. Jen, *Functional fullerenes for organic photovoltaics*. Journal of Materials Chemistry, *22(10)*, p. 4161-4177 (2012).
9. He, D., *et al.*, *A highly efficient fullerene acceptor for polymer solar cells*. Physical Chemistry Chemical Physics, *16(16)*, p. 7205-7208 (2014).
10. Mahmood, A., *et al.*, *A novel thiazole based acceptor for fullerene-free organic solar cells*. Dyes and Pigments, *149*, p. 470-474 (2018).
11. Mahmood, A., *et al.*, *Introducing Four 1,1-Dicyanomethylene-3-indanone End-Capped Groups as an Alternative Strategy for the Design of Small-Molecular Nonfullerene Acceptors*. The Journal of Physical Chemistry C, *122(51)*, p. 29122-29128 (2018).
12. Xiao, B., *et al.*, *A comparison of n-type copolymers based on cyclopentadithiophene and naphthalene diimide/perylene diimides for all-polymer solar cell applications*. Polymer Chemistry, *6(43)*, p. 7594-7602 (2015).
13. Xiao, B., *et al.*, *Quinoxaline-Containing Nonfullerene Small-Molecule Acceptors with a Linear A2-A1-D-A1-A2 Skeleton for Poly(3-hexylthiophene)-Based Organic Solar Cells*. ACS Applied Materials & Interfaces, *10(12)*, p. 10254-10261 (2018).
14. Xiao, B., *et al.*, *Achievement of High Voc of 1.02 V for P3HT-Based Organic Solar Cell Using a Benzotriazole-Containing Non-Fullerene Acceptor*. Advanced Energy Materials, *7(8)*, p. 1602269 (2017).
15. Li, J., *et al.*, *A thieno[3,4-b]pyrazine-based A2–A1–D–A1–A2 type low bandgap non-fullerene acceptor with 1,1-dicyanomethylene-3-indanone (IC) as the terminal group*. Journal of Materials Chemistry C, *7(29)*, p. 8820-8824 (2019).
16. Tang, A., *et al.*, *Benzotriazole-Based Acceptor and Donors, Coupled with Chlorination, Achieve a High VOC of 1.24 V and an Efficiency of 10.5% in Fullerene-Free Organic Solar Cells*. Chemistry of Materials, *31(11)*, p. 3941-3947 (2019).
17. Chen, Y., *et al.*, *Benzotriazole-Based p-Type Polymers with Thieno[3,2-b]thiophene ð-Bridges and Fluorine Substituents To Realize High VOC*. ACS Applied Polymer Materials, *1(4)*, p. 906-913 (2019).
18. Li, J., *et al.*, *The first thieno[3,4-b]pyrazine based small molecular acceptor with a linear A2–A1–D–A1–A2 skeleton for fullerene-free organic solar cells with a high Voc of 1.05 V*. Chemical Communications, *54(76)*, p. 10770-10773 (2018).
19. Tian, H., *et al.*, *A Triphenylamine Dye Model for the Study of Intramolecular Energy Transfer and Charge Transfer in Dye-Sensitized Solar Cells*. Advanced Functional Materials, *18(21)*, p. 3461-3468 (2008).
20. Lincker, F., *et al.*, *Fluorenone-Based Molecules for Bulk-Heterojunction Solar Cells: Synthesis, Characterization, and Photovoltaic Properties*. Advanced Functional Materials, *18(21)*, p. 3444-3453 (2008).
21. Cho, N., *et al.*, *Synthesis and characterization of push–pull organic semiconductors with various acceptors for solution-processed small molecule organic solar cells*. Tetrahedron, *68(21)*, p. 4029-4036 (2012).
22. Yassar, A., C. Videlot, and A. Jaafari, *Synthesis and photovoltaic properties of mono-substituted quaterthiophenes bearing strong electron-withdrawing group*. Solar Energy Materials and Solar Cells, *90(7)*, p. 916-922 (2006).
23. Li, Y., *et al.*, *Novel low-bandgap oligothiophene-based donor-acceptor alternating conjugated copolymers: Synthesis, properties, and photovoltaic applications*. Journal of Polymer Science Part A: Polymer Chemistry, 48(13), p. 2765-2776 (2010).
24. Li, W., *et al.*, *D-A-π-A Featured Sensitizers Bearing Phthalimide and Benzotriazole as Auxiliary Acceptor: Effect on Absorption and*

Charge Recombination Dynamics in Dye-Sensitized Solar Cells. ACS Applied Materials & Interfaces, *4(3),* p. 1822-1830 (2012).

25. Li, Z., *et al., Design and synthesis of solution processable small molecules towards high photovoltaic performance.* Journal of Materials Chemistry, *21(7),* p. 2159-2168 (2011).
26. Pai, C.L., *et al., Electronic structure and properties of alternating donor–acceptor conjugated copolymers: 3,4-Ethylenedioxythiophene (EDOT) copolymers and model compounds.* Polymer, *47(2),* p. 699-708 (2006).
27. Skabara, P.J., *et al., Fluorene functionalised sexithiophenes—utilising intramolecular charge transfer to extend the photocurrent spectrum in organic solar cells.* Journal of Materials Chemistry, *17(11):* p. 1055-1062 (2007).
28. Lee, J.Y., *et al., Synthesis of random copolymers based on 3-hexylthiophene and quinoxaline derivative: Influence between the intramolecular charge transfer (ICT) effect and π-conjugation length for their photovoltaic properties.* Synthetic Metals, *161(1),* p. 1-6 (2011).
29. Jung, I.H., *et al., Synthesis and characterization of fluorene and cyclopentadithiophene-based copolymers exhibiting broad absorption for photovoltaic devices.* Journal of Polymer Science Part A: Polymer Chemistry, *49(5),* p. 1248-1255 (2011).
30. Kim, Y.G., *et al., Variable band gap conjugated polymers for optoelectronic and redox applications.* Journal of Materials Research, *20(12),* p. 3188-3198 (2005).
31. Cheng, Y.J., *et al., Alternating copolymers incorporating cyclopenta[2,1-b:3,4-b2] dithiophene unit and organic dyes for photovoltaic applications.* Journal of Polymer Science Part A: Polymer Chemistry, *49(8),* p. 1791-1801 (2011).
32. Li, Y., *et al., Molecular structure–property engineering for photovoltaic applications: Fluorene-acceptor alternating conjugated copolymers with varied bridged moieties.* Polymer, *51(8),* p. 1786-1795 (2010).
33. Jung, I.H., *et al., Synthesis and Photovoltaic Properties of Cyclopentadithiophene-Based Low-Bandgap Copolymers That Contain Electron-Withdrawing Thiazole Derivatives.* Chemistry – A European Journal, *16(12):* p. 3743-3752 (2010).
34. Ranjith, K., *et al., Dithienylcyclopentadienone derivative-co-benzothiadiazole: An alternating copolymer for organic photovoltaics.* Solar Energy Materials and Solar Cells, *98,* p. 448-454 (2012).
35. Li, Y., *et al., Energy Level and Molecular Structure Engineering of Conjugated Donor" Acceptor Copolymers for Photovoltaic Applications.* Macromolecules, *42(13),* p. 4491-4499 (2009).
36. Han, G., *et al., Terminal π–π stacking determines three-dimensional molecular packing and isotropic charge transport in an A–π–A electron acceptor for non-fullerene organic solar cells.* Journal of Materials Chemistry C, *5(20),* p. 4852-4857 (2017).
37. Mai, J., *et al., Hidden Structure Ordering Along Backbone of Fused-Ring Electron Acceptors Enhanced by Ternary Bulk Heterojunction.* Advanced Materials, *30(34),* p. 1802888 (2018).
38. Li, M., *et al., Tuning the dipole moments of nonfullerene acceptors with an asymmetric terminal strategy for highly efficient organic solar cells.* Journal of Materials Chemistry A, *7(15),* p. 8889-8896 (2019).
39. Li, C., *et al., A nonfullerene acceptor utilizing a novel asymmetric multifused-ring core unit for highly efficient organic solar cells.* Journal of Materials Chemistry C, *6(18),* p. 4873-4877 (2018).
40. Yin, S., *et al., Balanced Carrier Transports of Electrons and Holes in Silole-Based CompoundsA Theoretical Study.* The Journal of Physical Chemistry A, *110(22),* p. 7138-7143 (2006).
41. Troisi, A. and G. Orlandi, *The hole transfer in DNA: calculation of electron coupling between close bases.* Chemical Physics Letters, *344(5),* p. 509-518 (2001).